Eur. Phys. J. B **14**, 281–286 (2000)

THE EUROPEAN PHYSICAL JOURNAL B

EDP Sciences

Electronic structure of $LiMnO_2$: X-ray emission and photoelectron spectra and band structure calculations

V.R. Galakhov[1,a], M.A. Korotin[1], N.A. Ovechkina[1], E.Z. Kurmaev[1], V.S. Gorshkov[2], D.G. Kellerman[2], S. Bartkowski[3], and M. Neumann[3]

[1] Institute of Metal Physics, Russian Academy of Sciences – Ural Division, 620219 Yekaterinburg GSP-170, Russia
[2] Institute of Solid State Chemistry, Russian Academy of Sciences – Ural Division, 620219 Yekaterinburg GSP-145, Russia
[3] University of Osnabrück – Fachbereich Physik, 49069 Osnabrück, Germany

Received 15 March 1999 and Received in final form 14 July 1999

Abstract. The electronic structure of $LiMnO_2$ and Li_2MnO_3 was studied by means of X-ray photoelectron and soft X-ray emission spectroscopy. For $LiMnO_2$, LSDA and LSDA+U calculations were carried out. The LSDA+U calculations are in rather good agreement with the measured valence-band structure as well as with the magnetic and electrical properties of $LiMnO_2$. It is shown that the band gap in $LiMnO_2$ is determined by the *charge-transfer* effect.

PACS. 71.20.-b Electron density of states and band structure of crystalline solids – 78.70.En X-ray emission spectra and fluorescence – 79.60.-i Photoemission and photoelectron spectra

1 Introduction

Interest in the electronic structure of manganites was initiated by the discovery of colossal magnetoresistance effects in $R_{1-x}A_xMnO_3$, where R and A are rare-earth and alkaline-earth ions, respectively [1,2]. The most important application of $LiMnO_2$ is the usage for Li-batteries.

Pure $LaMnO_3$ is an antiferromagnetic insulator and exhibits a strongly Jahn-Teller (JT) distorted orthorhombic structure with an additional rotation of the oxygen octahedra. The doped compounds are typically ferromagnetic metals below the Curie temperature and show semiconducting behavior above it.

The Mn ions in $LiMnO_2$ have a formal valence of 3+, as in $LaMnO_3$. In this respect $LiMnO_2$ and $LaMnO_3$ can be considered as related compounds.

$LiMnO_2$ belongs to the space group $Pmmn$ (No 59) with the structural parameters $a = 2.8043 \pm 0.0006$ Å, $b = 4.5793 \pm 0.0012$ Å and $c = 5.7510 \pm 0.0011$ Å [3–5]. Its structure consists of three layers of MnO_2 separated by sheets of Li ions (see Fig. 1). Antiferromagnetic behavior was observed below $T_N = 300$ K with $\theta = -660$ K, and a Curie-Weiss moment of 4.91 μ_B, consistent with high-spin Mn^{3+} ions ($t_{2g}^3 e_g^1$) [6].

The oxide Li_2MnO_3 has the space group $C2/m$ with $a = 4.937(1)$ Å, $b = 8.532(1)$ Å, $c = 5.030(2)$ Å and $\beta = 109.46(3)°$ [7]. Below the Néel temperature of 36.5 K [7] it shows an antiferromagnetic behavior, and above the Néel temperature it is paramagnetic with a Curie-Weiss moment of 3.83 μ_B [8]. The Mn^{4+} ions in Li_2MnO_3 should have a $3d^3$ electron configuration, as in $CaMnO_3$ or $SrMnO_3$, with 3 electrons in t_{2g} orbitals.

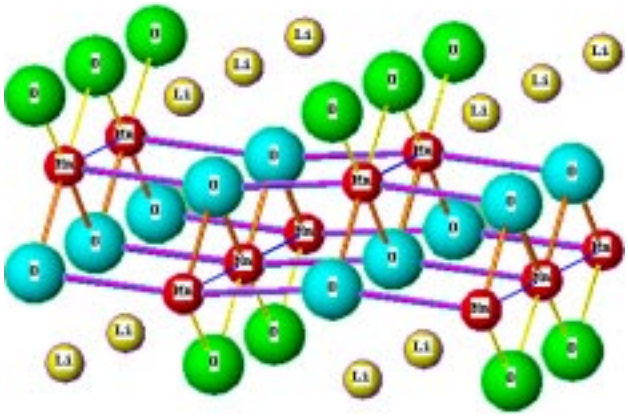

Fig. 1. Fragment of the crystal structure of $LiMnO_2$.

De Groot [9] studied X-ray Mn 2p and O 1s absorption spectra of $LiMnO_2$ and Li_2MnO_3. On the basis of the Mn 2p XAS measurements, de Groot [9] concluded, that in $LaMnO_3$ a high-spin ^5E ground state is realized, whereas the ground state of $LiMnO_2$ is a mixture of the high-spin ^5E and low-spin $^3T_1$ configurations. Recently, Singh [10] reported band structure calculations of $LiMnO_2$ using a local spin density approximation (LSDA).

Saitoh *et al.* [11,12] have analyzed Mn 2p XPS spectra of $LaMnO_3$ and $SrMnO_3$ on the basis of a configuration-interaction cluster model using the parameters of the $d-d$

[a] e-mail: GALAKHOV@ifmlrs.uran.ru

Coulomb interaction $U_{\rm eff}$ equal to 6.8 and 7.1 eV for $LaMnO_3$ and $SrMnO_3$, respectively. The *ligand* $p \rightarrow$ *transition metal* d charge-transfer energies $\Delta_{\rm eff}$ were equal to 1.8 eV for $LaMnO_3$ and -0.2 eV for $SrMnO_3$. For both $LaMnO_3$ and $SrMnO_3$ $U_{\rm eff}$ is larger than $\Delta_{\rm eff}$, which means that these compounds should be *charge-transfer* insulators. On the other hand, Chainani, Mathew, and Sarma [13] obtained for $LaMnO_3$ $\Delta = 5.0$ eV and $U = 4.0$ eV, and suggested that $LaMnO_3$ shows *Mott-Hubbard* rather than *charge-transfer* behavior. Note, that band-structure calculations of $LaMnO_3$ show a small gap at the Fermi level due to a Jahn-Teller splitting of the e_g band [14–17]. So, $LaMnO_3$ should be classified as a *Bloch–Wilson* insulator.

Here we give new experimental results of $LiMnO_2$ in comparison with Li_2MnO_3 obtained by X-ray photoelectron (XPS) and X-ray emission (XES) spectroscopic studies. For $LiMnO_2$, band-structure calculations in the frame of the LSDA and LSDA+U approximations have been carried out. We show that the band gap in $LiMnO_2$ is determined by the *charge-transfer* effect and not by the *Jahn-Teller* effect.

2 Experimental

Polycrystalline samples of $LiMnO_2$ and Li_2MnO_3 were prepared by solid-state reaction. Sintered mixtures of appropriate molar quantities of Mn_2O_3 and Li_2CO_3 were annealed at 750 °C for 20 h in helium. The specimens were checked by X-ray phase analysis using a DRON-2 diffractometer with Cu $K\alpha$ radiation.

X-ray photoelectron spectra were measured on an ESCA spectrometer from Physical Electronics (PHI 5600 ci) using monochromatic Al $K\alpha$ radiation. The specimens were investigated after breaking in vacuum. The spectra were calibrated using an Au-foil ($E_{\rm B}(4f_{7/2})$=84.0 eV). The energy resolution as determined at the Fermi level of the Au-foil was approximately 0.4 eV.

Mn $L\alpha$ ($3d4s \rightarrow 2p_{3/2}$ transitions), and O $K\alpha$ ($2p \rightarrow 1s$ transitions) X-ray emission spectra (XES) were measured on an RSM-500 X-ray spectrometer using electron excitation. The Mn L_α spectra were recorded in the second reflection order with an energy resolution of about 1 eV. The O $K\alpha$ spectra were measured in the first reflection order with a resolution of 1.3 eV. In order to calibrate the Mn $L\alpha$ and O $K\alpha$ emission spectra we used the $L\alpha$ spectra of pure Mn and V (E =637.4 and 511.3 eV, respectively). The X-ray tube was operated at V=4 keV and i=0.3 mA. The X-ray emission spectra were brought to the scale of the binding energies with respect to the Fermi level using the binding energies of the relevant initial (core-level) states of the X-ray transitions as measured by the XPS technique.

3 Computational details

The calculations of the electronic structure of $LiMnO_2$ were made using the structural data from [3,4]. The positions of atoms and empty spheres (es) added in the calculations, together with the radii of the muffin-tin (mt) spheres, are presented in Table 1. Each Mn atom is surrounded by a distorted oxygen octahedron in which both Mn–O distances and O–Mn–O angles are different. The distances between Mn and O in the octahedron are 1.89, 1.95 and 2.30 Å.

Table 1. Atomic positions and mt-radii in $LiMnO_2$.

site	atom	x	y	z	r(a.u.)
2*a*	Mn	0.25	0.25	0.6347	2.32
2*a*	Li	0.25	0.25	0.126	2.64
2*b*	O_1	0.25	0.75	0.144	1.83
2*b*	O_2	0.25	0.75	0.602	1.97
4*e*	es_1	0.25	0.00	0.397	1.64
4*e*	es_2	0.25	0.01	−0.136	1.44

Taking into account the simplest antiferromagnetic arrangement of the spins of the nearest (along the "*b*" crystallographic direction) Mn atoms, the space group becomes a $Pmm2$ one. The number of atoms per unit cell remains the same. The band structure calculations were made both in the local spin-density (LSDA) and LSDA+U approximations in the frame of the tight-binding linear muffin-tin orbitals scheme in atomic sphere approximation (TB-LMTO-ASA [18]; modified version 47 of the Stuttgart codes).

4 Results and discussion

In Table 2, the core-level binding energies and the maxima of the X-ray emission spectra for $LiMnO_2$ and Li_2MnO_3 are presented. The O 1s binding energy for Li_2MnO_3 is not expected to be chemically shifted and the shift of about 0.8 eV relative to $LiMnO_2$ can be explained as a shift of the Fermi level in the band gap. It is seen, that for Li_2MnO_3 with Mn^{4+} ions, the Mn 2p binding energies are 1.5 eV higher than for $LiMnO_2$ which contains Mn^{3+} ions. The Mn 2p core-level shift for Li_2MnO_3 in comparison with $LiMnO_2$ cannot be explained only by the shift of the Fermi level and but also by a "chemical shift" of 0.7 eV.

Figure 2a shows Mn 2p spectra of MnO, $LiMnO_2$ and Li_2MnO_3. The analysis of the spectrum of MnO is presented elsewhere (see, for example [19]).

Mn 2p core-level spectra of $LiMnO_2$ and Li_2MnO_3, were not studied before. The spectra exhibit satellites at energies of about 663 eV for $LiMnO_2$ and of 667 eV for Li_2MnO_3. In order to explain the satellite structure, let us use the interpretation of the Mn 2p spectra of $LaMnO_3$ and $SrMnO_3$ which have also Mn^{3+} and Mn^{4+} ions and may be considered as analogs of $LiMnO_2$ and Li_2MnO_3, respectively. The distances between the main peaks and the satellites for $LiMnO_2$ and Li_2MnO_3 are the same as for $LaMnO_3$ and for $SrMnO_3$, respectively (see Ref. [20]). According to the estimation of the Mn 2p spectra for $LaMnO_3$ [11], the main peaks of the spectrum of $LiMnO_2$ should arise from $\underline{p}d^5\underline{L}$ states whereas the satellites should

Table 2. Binding energies, values of the XPS Mn 3*s* splitting and energies of the maxima of the X-ray emission spectra (eV). All values are given with an accuracy of ±0.1 eV.

Oxide	Mn $2p_{3/2}$	O 1*s*	ΔE_{Mn3s}	Mn $L\alpha$	O $K\alpha$	Mn 3*d* (XES)	O 2*p* (XES)
$LiMnO_2$	641.5	529.4	5.4	638.2	525.2	3.3	4.2
Li_2MnO_3	643.0	530.2	4.5	638.8	525.9	4.2	4.3

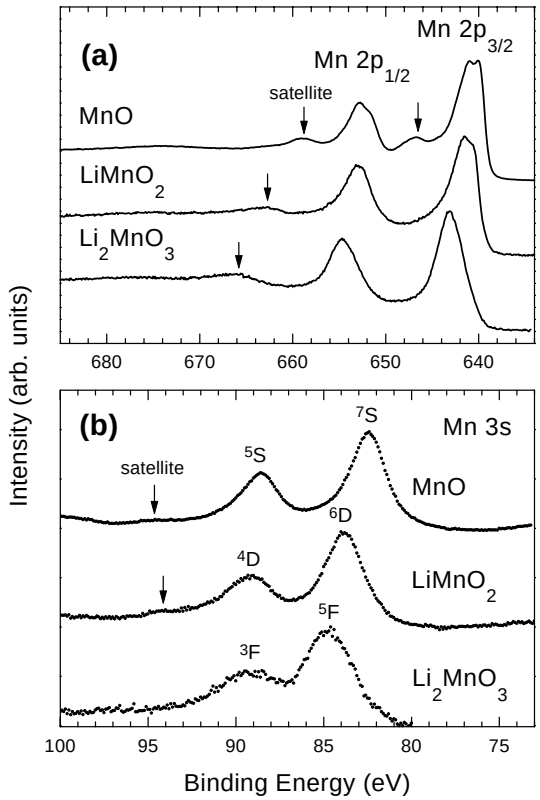

Fig. 2. (a) Mn $2p_{3/2}$ and $2p_{1/2}$ X-ray photoelectron spectra of MnO, $LiMnO_2$ and Li_2MnO_3. Arrows mark positions of satellites. For MnO, both the satellites for Mn $2p_{3/2}$ and $2p_{1/2}$ lines are shown. (b) Mn 3*s* X-ray photoelectron spectra of MnO, $LiMnO_2$ and Li_2MnO_3. Spin states for each oxide are shown. Arrows mark positions of satellites for MnO and $LiMnO_2$.

originate from $\underline{p}d^4$ and $\underline{p}d^6\underline{L}^2$ states. The oxide Li_2MnO_3 is an analog of $SrMnO_3$ and, similar to $SrMnO_3$ [11], the main peak consists of mixed $\underline{p}d^4\underline{L}$–$\underline{p}d^5\underline{L}^2$ states, while the satellite structure should be primarily due to $\underline{p}d^5\underline{L}^2$ states. Here, $\underline{L}$ denotes a ligand hole arising after the transfer of an electron from a 2*p* ligand level to a metal 3*d* level and $\underline{p}$ is a metal 2*p* hole in the final state of the photoemission process. Note, that the satellite structure accompanying the Mn $2p_{3/2}$ peak overlaps somewhat the Mn $2p_{1/2}$ peak.

The 3*s* core-level spectra of the 3*d* transition metals are known to exhibit exchange splitting. The magnitude of the splitting is proportional to $(2S + 1)$, where S is the local spin of the 3*d* electrons in the ground state. In addition to the exchange interaction between the 3*d* and 3*s* states, a *charge-transfer* process must be taken into account. For Cu-oxides, the *charge-transfer* effect dominates the *multiplet* effect in the 3*s* spectra [21]. As the number of *d* electrons decreases, the role of charge-transfer processes becomes less important and in Mn compounds the 3*s* splitting is determined mainly by exchange processes [22,23].

Figure 2b shows the Mn 3*s* X-ray photoelectron spectra of MnO, $LiMnO_2$, and Li_2MnO_3. All the spectra exhibit two sharp peaks which originate from the exchange interaction of the Mn 3*s* and Mn 3*d* electrons. The weak satellites, which have a charge-transfer character as in the case of the Mn 2*p* spectra are also present at the binding energy of about 94.5 eV for MnO and at 94 eV for $LiMnO_2$. The satellite is absent in the case of Li_2MnO_3. The satellite structure in the 3*s* spectra must be interpreted as for the 2*p* spectra. Note, that the distance *"main line–satellite"* for the 3*s* spectra is not the same as for the 2*p* spectra since the parameter U_{cd} (the core-hole *d* electron Coulomb attraction energy) in the case of the 3*s* spectra is about 1 eV less than the parameter for the 2*p* spectra [24].

The value of the Mn 3*s* splitting for $LiMnO_2$ is in between the values for compounds with Mn^{2+} and Mn^{4+} ions: MnO and Li_2MnO_3. The parameter of the exchange splitting is well correlated to the spin magnetic moment predicted for Mn^{3+}. Our measurements of the Mn 3*s* exchange splitting of $LiMnO_2$ indicate, that the ground state configuration of $LiMnO_2$ is the high-spin $3d^4$ one. No contribution of the low-spin configuration is detectable.

The conventional LSDA calculations of the antiferromagnetic $LiMnO_2$ compound predict a metallic ground state with a low value of the density of states (DOS) at the Fermi level: 0.61 states/(Ry×cell) and a Mn *d*-magnetic moment equal to 3.45 μ_B. The total and partial DOS's are shown in Figure 3a. Two positions of oxygen atoms are presented: O(1) and O(2). The inclusion of electron-electron correlations into the calculations in the frame of the LSDA+U calculations [25] with the parameters U and J, equal to 3.5 and 0.8 eV, respectively, leads to an insulating ground state with an energy gap of 1.31 eV and a Mn 3*d*-magnetic moment of 3.67 μ_B. The corresponding DOS curves are also presented in Figure 3b.

Singh [10] carried out band-structure calculations for $LiMnO_2$ using the LSDA approximation and received band gaps of 35 meV and 0.6 eV for ferromagnetically and antiferromagnetically ordered $LiMnO_2$, respectively. According to his calculations, in antiferromagnetic $LiMnO_2$ the O 2*p* and Mn 3*d* states are separated from each other. The Mn 3*d* states are narrow and are weakly hybridized with the O 2*p* states.

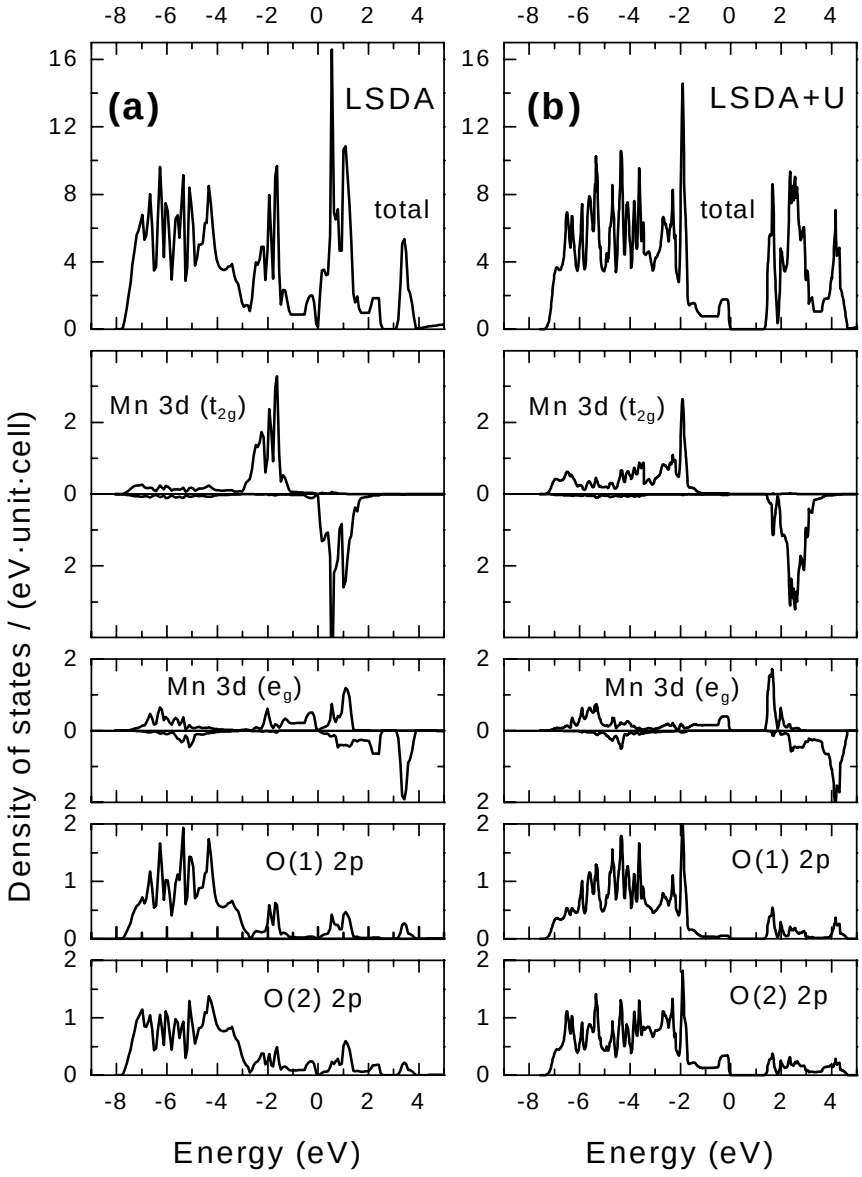

Fig. 3. (a) Total and partial (in the local coordinate system) densities of states obtained in the LSDA calculations. (b) Total and partial (in the local coordinate system) densities of states obtained in the LSDA+U calculations.

This discrepancy between the results of our calculations and those made by Singh can be explained by the difference in the crystal structure of $LiMnO_2$ used in the calculations. Singh has used a monoclinic modification of $LiMnO_2$ (space group $C2/m$, No 12). This structure represents a monoclinic deformation of α-$NaFeO_2$ [26]. Our calculations were carried out for $LiMnO_2$ in the orthorhombic structure (space group $Pmmn$).

It is known, that the band gap in the oxide $LaMnO_3$ is caused by the *Jahn-Teller* effect, and without the Jahn-Teller distortion (*i.e.* for a cubic cell), $LaMnO_3$ would be a ferromagnetic metal rather than an antiferromagnetic insulator. The splitting of the e_g bands due to the Jahn-Teller distortion leads to a small gap of the order of 0.1 eV. The electronic structure of $LaMnO_3$ can be rather well described by band-structure calculations, without taking into account electron-electron correlations [14–17]. For $LiMnO_2$, the value of the Jahn-Teller distortion is smaller than in $LaMnO_3$ and cannot split the e_g states and open the band gap. The dominant process of the formation of the band gap is the *charge-transfer* process.

Let us compare the band-structure calculations with the experimental X-ray photoelectron and emission spectra. Figure 4a shows the valence band X-ray photoelectron spectrum, the Mn $L\alpha$ and O $K\alpha$ X-ray emission spectra, and the partial densities of occupied (spin-up and spin down) states calculated in the LSDA+U approximation. The X-ray emission spectra are arranged with respect to the Fermi level, taking into account the Mn $2p_{3/2}$ and

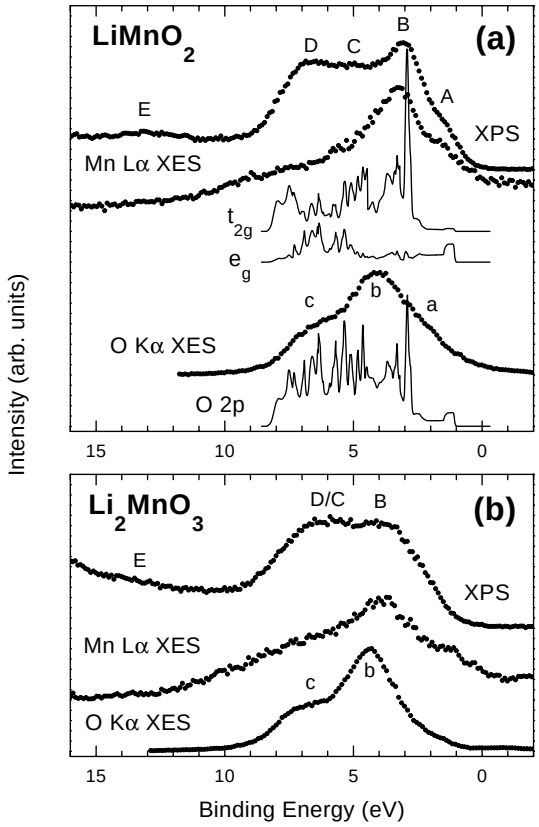

Fig. 4. (a) X-ray photoelectron spectrum of the valence band and Mn $L\alpha$ and O $K\alpha$ X-ray emission spectra of $LiMnO_2$, compared with the partial densities of states calculated using the LSDA + U approximation. (b) X-ray photoelectron spectrum of the valence band and Mn $L\alpha$ and O $K\alpha$ X-ray emission spectra of Li_2MnO_3. X-ray emission spectra are brought to a common energy scale using the core-level binding energies.

O 1s core-level binding energies measured by means of X-ray photoelectron spectroscopy (see Tab. 2).

According to the cluster-model analysis of $LaMnO_3$, the XPS region from 0 to 10 eV (features "A–D") of $LiMnO_2$ corresponds to the Mn $3d^4\underline{L}$ final-state configuration, while the satellite "E" at about 13 eV has strongly mixed d^3–$d^5\underline{L}^2$ character [11].

For the Al $K\alpha$ excitation, the cross-section ratio $\sigma(\mathrm{O}\ 2p) : \sigma(\mathrm{Mn}\ 3d)$ is equal to 0.17 : 1 [27] and as a consequence, the main contribution to the XPS valence-band spectrum in the presented energy region results from Mn 3d states. Therefore we compare the X-ray photoelectron and Mn $L\alpha$ spectra with the Mn 3d partial densities of states. The densities of states were shifted by hand until a good agreement with the experimental spectra was obtained. The general width and the shape of the photoelectron spectrum agree well with the calculated Mn 3d density of states. The maximum of the Mn $L\alpha$ emission spectrum coincides with the main peak "B" of the XPS valence-band spectrum at about 3 eV. The shoulder of the Mn $L\alpha$ spectrum at the energy of 5–10 eV is overlapping with the XPS peaks "C" and "D" at 5.5 and 7 eV, respectively.

According to the band-structure calculations, the shoulder "A" of the photoelectron spectrum near the Fermi level originates from e_g states. The feature of the Mn $L\alpha$ spectrum in the region from 0 to 2 eV is formed partly by a satellite which can be explained by multi-electron processes and partly by the Mn 3d (e_g) states. Peak "B" and feature "C" represent t_{2g} states. Feature "D" exhibits the sum of the t_{2g} and e_g states. Mn 3d states are also presented in the O $K\alpha$ spectrum due to the strong hybridization between the Mn 3d and O 2p states. Feature "a" of the O $K\alpha$ X-ray emission spectrum can be attributed to the e_g component of the Mn 3d states hybridized with the O 2p states. Feature "b" is mostly the O 2$p\pi$ states bonded to the metal 3d states. Feature "c" is a result of the mixing of Mn 3d (e_g) states to the bonding O 2$p\sigma$ states and of the Mn 3d (t_{2g}) states to the O 2$p\pi$ states.

In Figure 4b, the valence-band X-ray photoelectron spectrum and the Mn $L\alpha$ and O $K\alpha$ X-ray emission spectra of the oxide Li_2MnO_3 are shown. The photoelectron spectrum differs from the one of $LiMnO_2$. The feature "A" is absent, and the maximum of the Mn $L\alpha$ spectrum is shifted from the Fermi level by about 1 eV in comparison with $LiMnO_2$. The peak "B" is less intensive than for $LiMnO_2$, and the shoulders "C" and "D" are now a common sub-band "C/D". The changes in the XPS spectrum are reflected also in the Mn $L\alpha$ X-ray emission spectrum. The intensity relation of the main maximum ("B" feature in the XPS) to the one of the shoulders "C/D" is decreased. The Mn 3d electrons of Li_2MnO_3 should have occupied xy, yz or xz orbitals (corresponding to t_{2g} orbitals in the cubic description), and empty $x^2 - y^2$ and z^2 orbitals (e_g orbitals in the cubic description).

In the cluster approximation, the features "B–D" should be presented, probably, as strongly mixed $d^3\underline{L}$–$d^4\underline{L}^2$ states, as in the case of $SrMnO_3$ [11]. The satellite "E" has, probably, mainly $d^4\underline{L}^2$ character [11].

The O $K\alpha$ spectrum shows the main maximum "b" and the shoulder "c" which represent antibonding and bonding O 2p states, respectively. The O 2p states of Li_2MnO_3 are less hybridized with the Mn 3d states in comparison with $LiMnO_2$, since the less localized Mn 3d (t_{2g}) states are bonded to the O 2$p\pi$ states in Li_2MnO_3.

The difference in the valence-band spectra of $LiMnO_2$ and Li_2MnO_3 cannot be explained only by differences in the Mn 3d ion configurations. The difference in the atomic structure of these compounds should be taken into account. In $LiMnO_2$, MnO_6 octahedra share corners, and thus strong 180° Mn–O–Mn interactions are possible, giving rise to a large d bandwidth. In Li_2MnO_3, the MnO_6 octahedra share edges which leads to 90° Mn–O–Mn interaction and to a reduced d bandwidth.

5 Conclusion

In summary, we have presented X-ray photoelectron and soft X-ray Mn $L\alpha$ and O $K\alpha$ emission spectra of $LiMnO_2$ and Li_2MnO_3. Binding energies of the Mn 3d and O 2p

states were determined. For $LiMnO_2$, *ab initio* LSDA and LSDA+U calculations were carried out and a strong O $2p$–Mn $3d$ hybridization is established. It was shown that LSDA calculations are not able to describe the electronic properties of $LiMnO_2$ and predict a metallic state for it. The LSDA+U calculations showed that $LiMnO_2$ is a semiconductor with a band gap of 1.31 eV. In contrast to $LaMnO_3$, the band gap is determined not by the *Jahn-Teller* effect but by the *charge-transfer* effect.

Financial supports from the joint DFG/RFBR project "Electron Structure of Strongly Correlated Oxide Systems" and the NATO Project (Grant No. HTECH. LG971222) are gratefully acknowledged.

References

1. R. von Helmot, J. Wecker, B. Holzapfel, L. Schultz, K. Samver, Phys. Rev. Lett. **71**, 2331 (1993).
2. S. Jin, T.H. Tiefel, M. McCormack, R.A. Fastnacht, R. Ramesh, L.H. Chen, Science **264**, 413 (1994).
3. W.D. Johnston, R.R. Heikes, J. Am. Chem. Soc. **78**, 3255 (1956).
4. R. Hoppe, G. Brachtel, M. Jansen, Z. Anorg. Allg. Chem. **417**, 1 (1975).
5. D.G. Kellerman, V.S. Gorshkov, V.G. Zubkov, V.A. Perelyaev, V.R. Galakhov, E.Z. Kurmaev, S. Uhlenbrock, M. Neumann, Russian J. Inorg. Chem. **42**, 914 (1997).
6. P.F. Bongers, Ph.D. thesis, University of Leiden, Leiden, The Netherlands, 1957.
7. P. Strobel, B. Lambert-Andron, J. Solid State Chem. **75**, 90 (1988).
8. M. Jansen, R. Hoppe, Z. Anorg. Allg. Chem. **397**, 279 (1973).
9. F.M.F. de Groot, Ph.D. thesis, University of Nijmegen, Nijmegen, The Netherlands, 1991.
10. D.J. Singh, Phys. Rev. B **55**, 309 (1997).
11. T. Saitoh, A.E. Bocquet, T. Mizokawa, H. Namatame, A. Fujimori, M. Abbate, Y. Takeda, M. Takano, Phys. Rev. B **51**, 13942 (1995).
12. T. Saitoh, A.E. Bocquet, T. Mizokawa, A. Fujimori, Phys. Rev. B **52**, 7934 (1995).
13. A. Chainani, M. Mathew, D.D. Sarma, Phys. Rev. B **47**, 15397 (1993).
14. I. Solovyev, N. Hamada, K. Terakura, Phys. Rev. B **53**, 7158 (1996).
15. T. Misokawa, A. Fujimori, Phys. Rev. B **54**, 5368 (1996).
16. I. Solovyev, N. Hamada, K. Terakura, Phys. Rev. Lett. **76**, 4825 (1996).
17. E.Z. Kurmaev, V.M. Cherkashenko, M. Neumann, S. Stadler, D.L. Ederer, Ya.M. Mukovskii, I.V. Solovyev, N.A. Ovechkina, V.R. Galakhov, A. Fujimori, M.M. Grush, T.A. Callcott, R.C. Perera, J. Electr. Spectr. Relat. Phen. **96**, 187 (1998).
18. O.K. Andersen, Phys. Rev. B **12**, 3060 (1975); O.K. Andersen, O. Jepsen, Phys. Rev. Lett. **53**, 2571 (1984).
19. G.-H. Gweon, J.-G. Park, S.-J. Oh, Phys. Rev. B **48**, 7825 (1993).
20. E.Z. Kurmaev, M.A. Korotin, V.R. Galakhov, L.D. Finkelstein, E.I. Zabolotzky, N.N. Efremova, N.I. Lobachevskaya, S. Stadler, D.L. Ederer, T.A. Callcott, L. Zhou, A. Moewes, S. Bartkowski, M. Neumann, J. Matsuno, T. Misokawa, A. Fujimori, J. Mitchell, Phys. Rev. B **59**, 12799 (1999).
21. T. Mizokawa, A. Fujimori, H. Namatame, K. Akeyama, N. Kosugi, Phys. Rev. B **49**, 7193 (1994).
22. K. Okada, A. Kotani, Techn. Rep. ISSP, Ser. A, No. 2541 (1992); K. Okada, A. Kotani, J. Phys. Soc. Jpn **61**, 4619 (1992); K. Okada, A. Kotani, B. Thole, J. Electr. Spectrosc. Relat. Phen. **58**, 325 (1992).
23. T. Uozumi, K. Okada, A. Kotani, R. Zimmermann, P. Steiner, S. Hüfner, Y. Tezuka, S. Shin, Techn. Rep. ISSP, Ser. A, No. 3144 (1996).
24. T. Uozumi, K. Okada, A. Kotani, R. Zimmermann, P. Steiner, S. Hüfner, Y. Tezuka, S. Shin, J. Electron Spectr. Relat. Phen. **83**, 9 (1997).
25. V.I. Anisimov, F. Aryasetiawan, A.I. Lichtenstein, J. Phys. Cond. Matter **9**, 767 (1997).
26. A.R. Armstrong, P.G. Bruce, Nature (London) **381**, 499 (1996).
27. J.J. Yeh, I. Lindau, Atomic Data and Nuclear Data Tables **32**, 1 (1985).